

## Fast Single Image Haze Removal Method for Inhomogeneous Environment Using Variable Scattering Coefficient

Rashmi Gupta<sup>1</sup>, Manju Khari<sup>1</sup>, Vipul Gupta<sup>1</sup>, Elena Verdú<sup>2</sup>, Xing Wu<sup>3</sup>, Enrique Herrera-Viedma<sup>4</sup> and Rubén González Crespo<sup>2,\*</sup>

<sup>1</sup>Ambedkar Institute of Advanced Communication Technologies and Research, New Delhi, 110031, India

<sup>2</sup>Escuela Superior de Ingeniería y Tecnología, Universidad Internacional de La Rioja, Logroño, 26006, Spain

<sup>3</sup>School of Computer Engineering and Science, Shanghai University, Shanghai, 200444, China

<sup>4</sup>Escuela Técnica Superior de Ingenierías Informática y de Telecomunicación, Universidad de Granada, Granada, 18071, Spain

\*Corresponding Author: Rubén González Crespo. Email: ruben.gonzalez@unir.net

Received: 10 February 2020; Accepted: 27 March 2020

**Abstract:** The images capture in a bad environment usually loses its fidelity and contrast. As the light rays travel towards its destination they get scattered several times due to the tiny particles of fog and pollutants in the environment, therefore the energy gets lost due to multiple scattering till it arrives its destination, and this degrades the images. So the images taken in bad weather appear in bad quality. Therefore, single image haze removal is quite a bit tough task. Significant research has been done in the haze removal algorithm but in all the techniques, the coefficient of scattering is taken as a constant according to the homogeneous atmosphere but in real time this does not happen. Therefore, this paper introduces a simple and efficient method so that the scattering coefficient becomes variable according to the inhomogeneous environment. Then, this research aims to remove the haze with the help of a fast and effective algorithm i.e., Prior Color Fading, according to the inhomogeneous environmental properties. Thereby, to filter the depth map, the authors used a weighted guided image filtering which removes the drawbacks of guided image filter. Afterwards the scattering coefficient is made variable according to the inhomogeneous atmosphere and then the Simple Color Balance Algorithm is applied so that the readability property of images can be increased. The proposed method tested on various general outdoor images and synthetic hazy images and analyzed on various parameters Mean Square Error (MSE), Root Mean Square Error (RMSE), Peak Signal to Noise Ratio (PSNR), Mean Structural Similarity (MSSIM) and the Universal Objective Quality Index (UQI). Experimental results for the proposed method show that the proposed approach provides better results as compared to the state-of-the-art haze removal algorithms.

**Keywords:** Image dehazing; scattering coefficient; simple color balance; inhomogeneous environment



This work is licensed under a Creative Commons Attribution 4.0 International License, which permits unrestricted use, distribution, and reproduction in any medium, provided the original work is properly cited.

## 1 Introduction

Images recorded in foggy and hazy weather can be corrupted by scattering of atmospheric particles, which decreases the contrast, changes the color, and transforms the features of images in such a way that are difficult to identify by human vision and some outdoor systems based on computer vision. Therefore image dehazing is an essential and significant issue that has been widely researched so that an improved and better algorithm can be formed to eliminate this issue. The purpose of image dehazing is to eliminate the effects of weather factors in order to enhance the visual effects of the images and provide benefits for post-processing.

Many and very diverse applications have emerged in the last years, which can benefit from improvements in image processing, such as those related to video surveillance [1], visual question answering [2], automatic image annotation [3,54], activity recognition [4], some specific to mobile devices as location recognition [5] and mobile visual recognition [6], intelligent vehicles [7], etc.

Consequently, many techniques on image processing and specifically on image dehazing have been developed over the past decade [8], as described in Section 2 of this paper. Given the nature and requirements of some applications (video surveillance, location recognition, etc.), simple and quick methods are preferred. Some of the dehazing techniques [9–11] use a physical model of the deteriorated images to restore them. The physical reasons that have caused the image degradation are studied and modelled, and an inverse model is used to restore the image. The present research is based on the method proposed by Zhu et al. [11] that uses a linear model for modeling the scene depth using the brightness and the saturation of the hazy image. The parameters of the linear model are learnt by a supervised learning method. Although this method is simple providing efficient and good dehazing results, as required by some applications, it presents the drawback of considering the atmospheric scattering coefficient as constant, while atmospheric conditions may not be homogeneous [11]. Besides, the guided image filter used in this method does not remove halo artifacts from the image. Another simple method is the one proposed by He et al. [12], which uses a dark channel prior algorithm but does not work when there are white objects in the scene.

Therefore, taking Zhu et al. [11] method as the base, we propose a new method that removes the haze according to the inhomogeneous environmental properties. Unlike other previous methods, which take the scattering coefficients to calculate the transmission map as constant, our method uses a variable scattering coefficient that adapts to inhomogeneous environments. The method is described in Section 3 of this paper. It is tested on various hazy images and compared with other simple methods as He et al. [12] and Zhu et al. [11]. In this paper Prior Color Fading method is used to remove the haze according to the inhomogeneous environmental properties. Afterwards the scattering coefficient is made variable according to inhomogeneous atmosphere using  $\beta = \beta' e^{-\alpha d(x)}$  where  $\beta' = 1$  and  $\alpha$  is a constant whose value is between 0 and 1 according to inhomogeneous atmosphere.

As shown in Section 4 of this paper, by using ground truth images and calculating common metrics, it is proved that the proposed method presents better image quality assessment parameters than the other ones.

## 2 Related Work

There are different approaches for image dehazing: image enhancement methods, image fusion methods and image restoration methods [8]. Image enhancement methods upgrade the image quality by strengthening the image contrast directly. These methods are classified as histogram equalization [13,47,48], the Retinex method and frequency domain enhancement method. The method based on equalization of histogram strengthens the hazy image contrast by increasing the dynamic range of the gray values. Histogram equalization is further divided into global histogram equalization and local histogram equalization [14–16,49–52]. Global histogram equalization is a simple method and is suitable for overall enhancement of

bright and dark images. This method is highly efficient but it is difficult to restore the optimal value for each local area. Local histogram equalization is suitable for processing of hazy images with changeable depth of field, but local block effects exist and there is a large calculation complexity. The algorithms that are based on Retinex [17–18] are currently being used in the field of image enhancement for applications such as removal of shadow and removal of haze. Its principal concept is based upon obtaining the reflection properties of the objects from the influence of light on the image and it provides a model for describing the color invariance. The Retinex method is further divided into two types: single-scale Retinex [19] and multi-scale Retinex [20]. In frequency domain transform method a high pass filter is used for image filtering to suppress low frequencies and enhance high frequencies. Frequency domain methods include homomorphic filtering [21], the wavelet transforms [22] and the curvelet transform [23–24].

Image fusion is the technique based on the integration of all the relevant information from multiple source channels into a single and high quality image. Fusion strategies maximize the extraction of information from each channel such that the image information utilization can be improved. In this method fusion can be done with multi spectral images [25] or with a single image [26–28,52]. Schaul et al. [25] propose a method for fusing a visible and also a near-infrared image, which belongs to the same image, to help in obtaining a de-hazed color image. This method does not require the detection of any haze and air-light. It does not require the generation of any depth image maps neither. Ancuti et al. [26] introduce a strategy that is based on a fusion technique that takes as inputs two adapted versions of the original image. These images are weighted with the help of specific maps such that high accurate haze-free results can be obtained.

Image restoration based methods explore the reason for image degradation and analyze the imaging scheme, then recover the scene by an inverse transformation. In this method, single-image de-hazing along with additional information can be done by knowing the information of the scene [9], user's interaction [29] or by machine learning methods [10,11,30,51]. In multi-image de-hazing methods, the depth or detailed information can also be estimated using two or more different images that belong to the same scene. The recovery principle used by this method can be divided into two categories: different polarization filters [31] and different weather conditions [31–36]. Specifically, Schechner et al. [31] present an approach that is able to work under different atmospheric and viewing conditions. In this method, the formation of the image is deeply analyzed and the polarization effects of atmospheric scattering were also taken into account. This method can even work with only two different images, which are captured using a polarizer at different orientations. In this research, video de-hazing technique is used. The flickering artifacts are reduced by making the transmission values temporally coherent in a de-hazed video sequence.

Single image de-hazing with prior knowledge methods are based on priors or constraints. These include the algorithm of Tan [37], which can maximize the local contrast with single image only, but easily results in over color saturation in images along with heavy haze. Fattal's [38] method uses independent component analysis and a Markov random field to dehaze the image. It can produce good results when there is sufficient color information while in cases where the original assumption stands invalid, it can fail. The method proposed by Kratz et al. [39] uses Factorial Markov random field to compute the depth map information. This method is able to recover haze free images along with fine details but the results that are derived are often over enhanced and may suffer from oversaturation. He's et al. [12] method is based upon the usage of the dark channel approach to make the hazy image haze free. This method is simple and keeps high fidelity of the natural scene, but it is invalid when there are white objects. Tarel and Hautiere method uses contrast based enhancement approach for removing the haze effects. It helps in simplification of the dehazing process and also helps in efficiency improvement but many of the parameters used in the algorithm cannot be adjusted adaptively [40]. Kim's et al. [41–42] method can keep the balance between contrast enhancement and information loss, but it is not suitable for image

dehazing with thick fog. Zhu et al. [43] propose a powerful technique for removal of haze from a single input image. The authors create a linear model for scene depth modelling of the hazy image and use supervised learning algorithms. With the help of these supervised learning algorithms, the depth information is recovered. Experimental results show that the approach is highly efficient. Li et al. [44] introduce weighted guided image filter (WGIF). WGIF is developed by incorporating edge-aware weighting into an existing guided image filter (GIF). The WGIF technique can be used for haze removal in a single image and enhancement of image details. Zhu et al. [11] propose a powerful method based on color attenuation prior to the creation of a linear model for scene depth of hazy images. In this method, a de-hazed image is formed which is based on the depth map, scattering coefficient and transmission map of hazy input image. This method is fast and achieves good results but it has some drawbacks. The scattering coefficient in this method is taken as constant assuming that the environment is homogeneous but this does not correspond to reality. Besides, the guided image filter used in this method does not remove halo artifacts from the image.

In [11] Zhu et al. shows the procedure of how a de-hazed image is formed, provided a hazy image as input. Taking this method as the base, we propose a new method that removes the haze according to the inhomogeneous environmental properties. Unlike other previous methods, which take the scattering coefficients to calculate the transmission map as constant, our method uses a variable scattering coefficient that adapts to inhomogeneous atmosphere conditions, showing better results experimentally.

### 3 Proposed Method

As above mentioned, Zhu et al. [11] propose a powerful method of color attenuation prior to the creation of a linear model for scene depth based on hazy images. This method runs fast and achieves good results but it has drawbacks as it depends on the scattering coefficient and depth map to achieve the transmission map, and the scattering coefficient is considered as a constant according to homogeneous atmosphere, but actually atmosphere is not homogeneous. The developed methods, which utilize the scattering coefficients to calculate the transmission map, take the coefficients as constant. In the present paper, the authors propose a method that makes the scattering coefficient variable according to inhomogeneous atmosphere.

The flowchart in Fig. 1 shows the proposed method. To eliminate the drawbacks of guided image filtering, a weighted guided image filter is used. The scattering coefficient is taken according to the inhomogeneous atmosphere and, after getting the haze free image, a simplest color balance algorithm is applied to increase the readability property of images. All the parts of the flowchart are detailed in the next sections.

#### 3.1 Atmospheric Scattering Model (AMS)

The Atmospheric Scattering Model (AMS) outlines the generation of the hazy image. The AMS is extensively applied in image and video processing. Narasimhan et al. [32–36] further derive this model.

The mathematical expression of this model is:

$$H_i(X) = J_h(X)T_m(X) + A_l(1 - T_m(X)) \quad (1)$$

$$T_m(X) = e^{-\beta D(X)} \quad (2)$$

where  $X$  is the image pixel's position,  $H_i$  is the hazy image,  $J_h$  is the haze free image,  $A_l$  is the atmospheric light,  $\beta$  is the atmospheric scattering coefficient,  $D$  is the scene depth, and  $T_m$  is the transmission map.

$H_i$ ,  $J_h$  and  $A_l$  are three dimensional (3D) vectors in the Red-Green-Blue (RGB) space. Our objective is to find  $D_X$ ,  $T_m(X)$  and  $A_l$  and then, from these results, to find the haze free image i.e.,  $J_h$ . This model helps in developing a relationship between the input which is a hazy image and the output which is a haze free image and the other described terms in the equations above. So, this is a fundamental model that creates haze free image with the help of a hazy image.

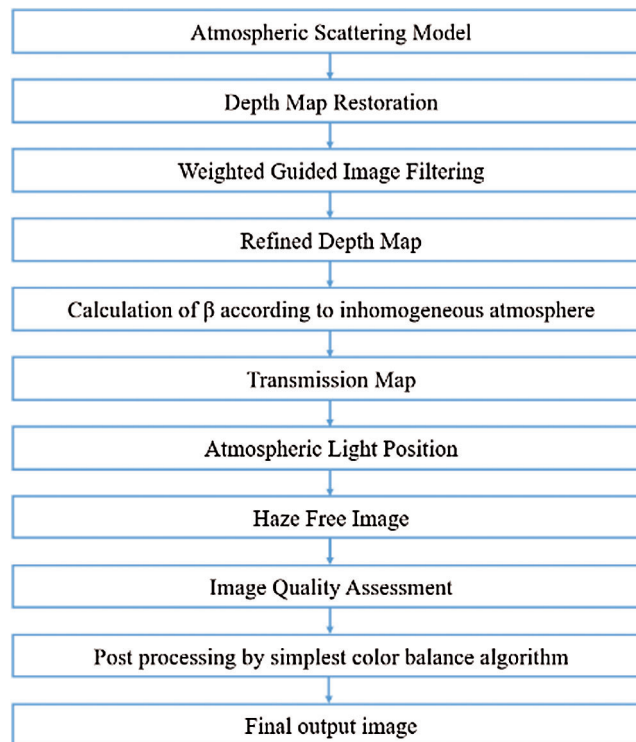


**Figure 1:** Proposed method flowchart

### 3.1.1 Concept of Light Propagation

The basic approach to capture an outdoor scene in camera is to just sense the reflected light from the scene to the camera sensor and project it on the imaging system. This process runs smoothly in sunny weather. But when the weather becomes hazy two mechanisms happen, one is the air light and the other one is direct attenuation (see Fig. 2). Direct attenuation is caused because the reflected energy gets reduced, which results in low brightness intensity. Direct attenuation can also be shown by the term  $J_h(X)T_m(X)$  in Eq. (1) of the atmospheric scattering model. This equation denotes the decrease in the pixel intensity of the images. This means the brightness will decrease under the influence of the direct attenuation. The term  $A_l(1 - T_m(X))$  in Eq. (1) is shown as air-light. Due to air-light, along with an increase in the brightness, there is a decrease in saturation. Air-light plays the main role to show the hazy regions that are characterized by low saturation and high brightness. Therefore it can be said that the density of the haze is directly proportional to the influence of air-light. Hence, this allows the utilization of the difference between the saturation and the brightness for the estimation of haze concentration [11].

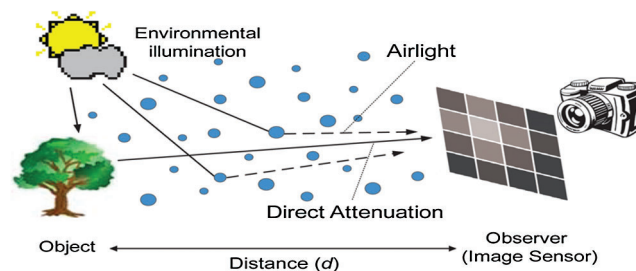


**Figure 2:** Light propagation model

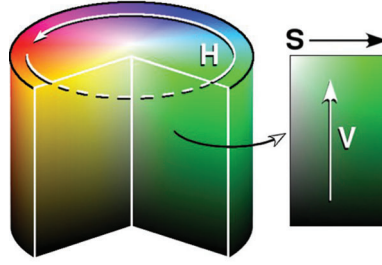


**Figure 3:** HSV color cylinder diagram

To find the saturation and brightness value of the image, the authors have used the HSV color space (see Fig. 3). HSV stands for (Hue, Saturation, Value). From this color space, the difference between saturation and brightness can be used to calculate the amount of haze occurrence in the image. We use these saturation and brightness values in a linear model for depth map restoration.

### 3.2 Depth Map Restoration

The variation between the saturation value and brightness value of the pixels gives the knowledge of DEPTH MAP as

$$D_X \propto C_X \propto (B_X - S_X) \quad (3)$$

where  $X$  is the image pixel's position,  $D$  is the scene depth,  $C$  is the haze concentration,  $B$  is the scene brightness, and  $S$  is the pixel saturation.

From the statistics obtained through different experiments on hazy images, color attenuation prior is found [11]. For example, a large value in saturation and a moderate level of brightness, with a difference between saturation value and brightness level near to zero, describe a haze free region. Also, it is observed that when the saturation value decreases gradually, the brightness level increases and their difference also increases, which shows a hazy region. If the difference increases more, it shows a dense hazy region. From these observations it can be concluded that these features (namely brightness level, saturation value and their difference) are subjected to deviate consistently in a hazy image.

#### 3.2.1 Linear Depth Map Restoration Model

The variation between the radiance (brightness) and iridescence (saturation) value of the pixels constitutes the concentration of haze. Therefore a linear model has been proposed to find the depth map. The map found from this model is called the RAW DEPTH MAP.

The mathematical equation for the above described model is as follows:

$$D(X) = a_0 + b_1 B(X) + c_2 S(X) + \varepsilon(X) \quad (4)$$

where  $X$  is the image pixel's position,  $D$  is the scene depth,  $B$  is the brightness (radiant) component of the hazy image,  $S$  is the saturation (iridescent) component and  $\varepsilon$  is the random variable of a random image which represents Gaussian density with mean value as zero and variable  $\sigma^2$ .

$a_0$ ,  $b_1$ ,  $c_2$  and the variable  $\sigma^2$  are the unknown coefficients, which are defined through 500 training samples used to produce this linear model and the leading observing outcome [11] is:  $a_0 = 0.121779$ ,  $b_1 = 0.959710$ ,  $c_2 = -0.780245$ ,  $\sigma = 0.041337$ . Upon finding the value of coefficients, these can be utilized for any single hazy image.

This model does not work in some selected situations like those scenes with white objects present in image, which usually have high brightness pixel values and low saturation pixel values. This model

assumes the scene objects with white colors as if they are distant objects and in turn will make erroneous depth map estimation in some instances.

For solving the above problem, it is required to account for all the pixels present in the neighborhood. On speculation, it was found out that the depth of the scene is constant locally, then the raw depth map is denoted by:

$$D_r(X) = \min_{y \in \Omega_r(X)} D(y) \quad (5)$$

where  $\Omega_r(X)$  is  $r \times r$  neighborhood centered at  $X$ ,  $D_r$  is the depth map with scale  $r$ . In [11]  $r = 15$  is considered as the appropriate value. To improve the Depth Map and for smoothening the image Weighted Guided Image Filtering has been used.

### 3.3 Weighted Guided Image Filtering

Weighted Guided Image Filtering (WGIF) is used for refining or smoothening the depth map. This filter comprises the properties of both local and global filters while the guided image filtering depends on the local filtering properties, and the local filtering techniques are affected by halo artifacts. An edge aware weighting is introduced and incorporated into the guided image filter. In reality, edges show effective and expressive information about the scene in the image. Therefore, the pixel edges have been assigned larger weights than pixels at flat areas. Therefore, WGIF avoids/reduces the halo artifacts like the global filters. WGIF carries complexity of  $O(N)$  for an image with  $N$  pixels. Therefore, WGIF is better than the guided image filter. The basic principle of this filter depends on the two images: the guidance image and the input image as shown in Fig. 4. The guidance image can be the own input image or any other reference image. With the help of these two images a linear model is created which helps to model a new smooth output image [44].

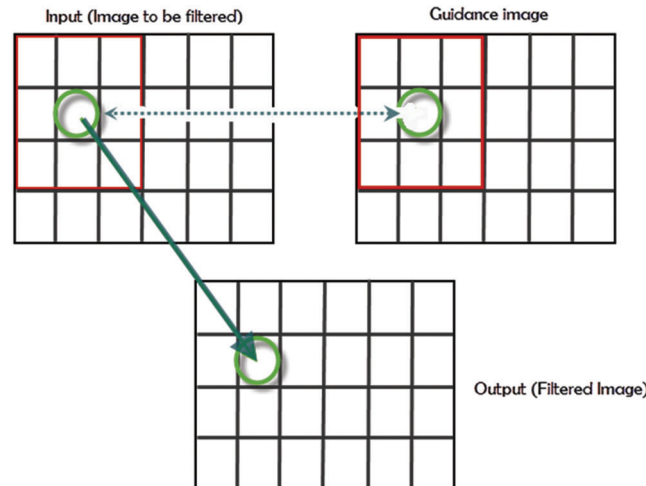


**Figure 4:** Basic function of guided image filter

### 3.4 Calculation of Scattering Coefficient According to Inhomogeneous Atmosphere

To calculate the scattering coefficient firstly we have to understand some points before the final formula can be derived:

- The scattering coefficient is a value that tells how much amount of light is scattered towards the camera which captures the image.
- Depth Map can be defined as an image or an image channel which contains information related to the distance of the surfaces of the scene objects from a view point.
- From the basics of depth map restoration model, depth map is directly proportional to the concentration of haze.

- According to the inhomogeneous or natural environment, the scattering coefficient decreases as the depth value increases and increases as the depth value decreases i.e.,

$$SCATTERING\ COEFFICIENT(\beta) \propto \frac{1}{DEPTH\ MAP(D(X))} \quad (6)$$

- According to Eq. (2), if  $D(X) = 0$ , then  $T_m(X) = 1$ , if  $D(X) = \infty$ ,  $T_m(X) = 0$ .

Therefore it can be said that, as depth value increases, transmission value decreases, i.e.,

$$T_m(X) \propto \frac{1}{D(X)} \quad (7)$$

Therefore from Eqs. (6) and (7), we can make a relation between  $\beta$  and  $d(x)$  i.e.,

$$\beta = \beta' e^{-\alpha d(x)} \quad (8)$$

$\beta' = 1$  and  $\alpha$  is a constant whose value is between 0 and 1.

Therefore from Eq. (8) the scattering coefficient behaves according to the inhomogeneous environment.

### 3.5 Atmospheric Light Position Estimation

To obtain the atmospheric light position firstly we have to analyze the atmospheric scattering model equations that are:

$$H_i(X) = J_h(X)T_m(X) + A_l(1 - T_m(X)) \quad (9)$$

$$T_m(X) = e^{-\beta D(X)} \quad (10)$$

If  $D(X) = \infty$  in Eq. (10),  $T_m(X)$  becomes zero i.e.,  $T_m(X) = 0$ . If  $T_m(X) = 0$  in Eq. (9) then we get a final expression i.e.,  $H_i(X) = A_l$ . This means that when depth map becomes infinite (very large) then we get the pixels which are brightest and these pixels from the hazy image are the position of atmospheric light.

So from the above discussion, we selected the peak 0.1% brightest pixels that are present in the depth map and selected the pixel that has the highest intensity in the sample hazy image  $H_i$  and this brightest pixel is considered as atmospheric light [11].

### 3.6 Transmission Map

From Eq. (2) the mathematical equation to find the transmission map is given as:

$$T_m(X) = e^{-\beta D(X)} \quad (11)$$

So from the above discussion we have found the depth map and the variable scattering coefficient according to inhomogeneous atmosphere and now just put these in the above equation and then we get the transmission map [11].

### 3.7 Output Haze Free Image

$J_h(X)$  belongs to the haze free image and here we can estimate or find the haze free image with the help of AMS. Now Eq. (1) is as follows:

$$J_h(X) = \frac{H_i(X) - A_l}{T_m(X)} + A_l = \frac{H_i(X) - A_l}{e^{-\beta D(X)}} + A_l \quad (12)$$

The final expression for obtaining the Haze free image  $J_h$  is expressed as:

$$J_h(X) = \frac{H_i(X) - A_l}{\min\{\max\{e^{-\beta D(X)}, 0.1\}, 0.9\}} + A_l \tag{13}$$

### 3.8 Image Quality Assessment

The digital image world is quickly making their way in our daily lives because huge amount of data or information is presented as visual signals. This data mostly flow across different types of stages to reach its destination. Some data processing stages for images as data are image acquisition, filtering, segmentation, compression and image transmission [53]. All these stages lead to introduce distortion in the images and degrade the quality of images. Therefore to preserve, control and strengthen the image quality, processing systems have to analyze the image quality at all stages.

Therefore, for measurement of the image quality, the main goal is to analyze the effects of different processing stages and then take possible measures for improving the image quality according to their needs. Fig. 5 provides a classification of assessment techniques that are detailed below.

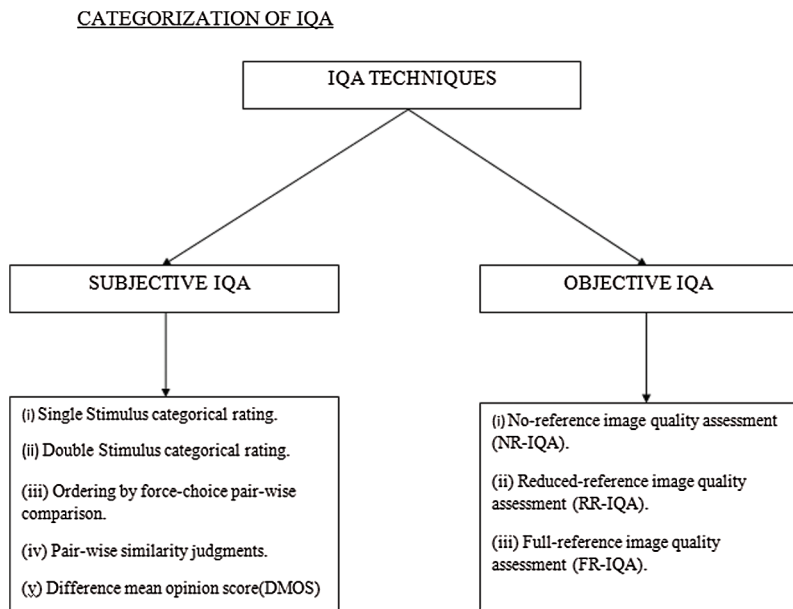


**Figure 5:** Classification of image quality assessment techniques

#### 3.8.1 Subjective Image Quality Assessment (S-IQA)

S-IQA is an exact and authentic way to analyze the quality of images. However, this method is expensive and time consuming. Therefore it is not possible to apply it in real world. Also this technique is affected by different factors such as viewing distance, lighting condition, display device, etc. Hence, it is essential to develop some mathematical models which are eligible to estimate the quality evaluation correctly.

#### 3.8.2 Objective Image Quality Assessment (O-IQA)

The O-IQA is framed as the mathematical models that estimate the quality of images precisely and automatically. This type of technique depends on the availability of a reference image, which should not contain distortion and the quality of the image must also be high. This technique is classified into three types, as follows:

1. Full Reference Image Quality Assessment Technique (FR-IQA)

## 2. Reduced Reference Image Quality Assessment (RR-IQA)

### 3. No Reference Image Quality Assessment (NR-IQA)

To analyze the quality of these research results the authors have used the FR-IQA in which a reference image is fully available which satisfies the criteria of O-IQA.

The parameters used in this project for measuring the image quality are: Mean Square Error (MSE), Root Mean Square Error (RMSE), Peak Signal-to-Noise Ratio (PSNR), Structural Similarity Index Method (SSIM) and Mean Structural Similarity Index Method (MSSIM), universal objective quality index.

MSE is defined as the power distortion which is shown by the difference between the test image and reference image.

Mathematical formula for MSE is:

$$MSE = \frac{1}{n * m} \sum_{j=1}^n \sum_{i=1}^m (I_r(i,j) - I_t(i,j))^2 \quad (14)$$

where  $n$  is the number of rows,  $m$  is the number of columns,  $I_r$  is the Reference image, and  $I_t$  is the test image.

RMSE can be simply denoted by:

$$RMSE = \sqrt{MSE} \quad (15)$$

PSNR is the ratio of maximum power of the signal to the power of distortion and is calculated as:

$$PSNR = 10 \log \left( \frac{D^2}{MSE} \right) \quad (16)$$

where  $D$  is the dynamic range of pixel intensities e.g., for an 8 bits/pixel in an image,  $D = 255$  [8].

SSIM algorithm is depending on the property of pixels. Pixels of image carry important information regarding the structure of a scene. Therefore, SSIM algorithm is able to measure the structural information change after the processing of an image through different stages.

The SSIM algorithm finds the similarity index measurement with the help of three steps (see Fig. 6): luminance comparison, contrast comparison and structure comparison [45].

The overall similarity measure,  $S(I_r, I_t)$ , is a function of  $l(I_r, I_t)$ ,  $c(I_r, I_t)$  and  $s(I_r, I_t)$ , where  $I_r$  is the reference image and  $I_t$  is the test image.

For luminance comparison we have:

$$l(I_r, I_t) = \frac{2\mu_r\mu_t + T_1}{\mu_r^2 + \mu_t^2 + T_1} \quad (17)$$

where  $T_1$  is a positive stabilizing constant,  $T_1 = (t_1L)^2$ ,  $t_1 \ll 1$ ,  $L$  is a dynamic range of pixel values,  $\mu$  is the mean intensity.

For contrast comparison we have:

$$c(I_r, I_t) = \frac{2\sigma_r\sigma_t + T_2}{\sigma_r^2 + \sigma_t^2 + T_2} \quad (18)$$

where  $T_2$  is a positive stabilizing constant,  $T_2 = (t_2L)^2$ ,  $t_2 \ll 1$ ,  $\sigma$  is the standard deviation as a round estimate of the signal contrast.

For structure comparison function we have:

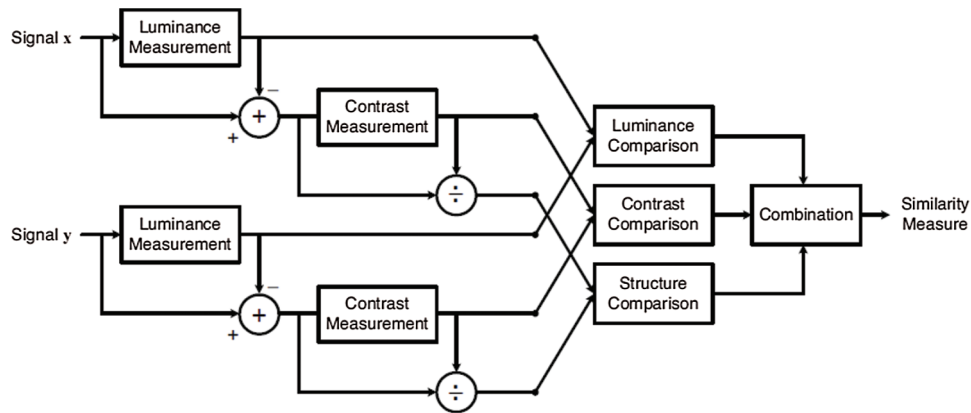


Figure 6: Similarity measurement flow diagram [8]

$$s(I_r, I_t) = \frac{\sigma_{r,t} + T_3}{\sigma_r \sigma_t + T_3} \tag{19}$$

where  $T_3$  is a positive stabilizing constant,  $\sigma_{r,t}$  is the correlation coefficient between the reference and test image.

Finally, SSIM is defined as:

$$SSIM(I_r, I_t) = [l(I_r, I_t)]^\alpha [c(I_r, I_t)]^\beta [s(I_r, I_t)]^\gamma \tag{20}$$

$\alpha$ ,  $\beta$  and  $\gamma$  are positive constants [45].

The mean structural similarity index (MSSIM) is given by:

$$MSSIM(I_r, I_t) = \frac{1}{M} \sum_{i=1}^M SSIM(I_r^i, I_t^i) \tag{21}$$

where  $M$  is the number of samples present in the quality map,  $I_r^i$  And  $I_t^i$  are image contents [45].

The calculation of the Universal Objective Quality Index (UQI) is easy and applicable to a variety of image processing applications. The designing of this index is done by modeling the distortion of an image as a combination of three factors: Loss of Correlation, Contrast Distortion and Luminance Distortion. This index is derived from the SSIM [46]. Since,

$$SSIM(I_r, I_t) = [l(I_r, I_t)]^\alpha [c(I_r, I_t)]^\beta [s(I_r, I_t)]^\gamma \tag{22}$$

$\alpha$ ,  $\beta$  and  $\gamma$  are positive constants. Therefore, UQI [46] is considered as a special case of SSIM index on satisfying these conditions:  $T_1 = T_2 = T_3 = 0$  and  $\alpha = \beta = \gamma = 1$ .

### 3.9 Post Processing of De-haze Image Using Simplest Color Balance Algorithm

Color balance is an important part of almost any image processing pipeline. It is defined as the global adjustments of all the intensities that are present in the primary colors i.e., red, green and blue. Color balance helps in altering the overall mixture of the colors that are present in an image and is used for color correction. Generally, the color of the objects remains the same but for the observer the color of the object changes under different illuminant conditions. Hence color balancing is a way to bring the ability to computers to make an object in an image has the same color even under different illuminants.

Some color balance algorithms are gray world algorithm, simplest color balance algorithm, robust auto white balance algorithm, or sensor correlation algorithm. In the present work, the authors have used the simplest color balance algorithm that is described as follows.

The simplest color balance algorithm increases the readability property of images. This algorithm produces white balance and contrast enhancement. The algorithm simply stretches the RGB values so that the lower intensity pixel occupies the calculated minimum possible value and the higher intensity pixels occupy the calculated maximum possible value. Simplest color balance saturates a certain percentage of the image's pixels to white, and dark pixels to black. The saturation level is an adjustable parameter that affects the quality of the output. This is the histogram based method [46].

### 3.10 Algorithm of the Proposed Method

The steps of the proposed algorithm are:

Step 1: Analyze the atmospheric scattering model using Eqs. (1) and (2).

Step 2: Restore the depth map using the linear depth map restoration model from Eq. (4).

Step 3: Refine the depth map using WGIF.

Step 4: Calculation of scattering coefficient according to inhomogeneous atmosphere using Eqs. (6) and (7). Eq. (8) is the scattering coefficient according to inhomogeneous environment.

Step 5: Estimate the position of atmospheric light by choosing the 0.1% brightest pixels present in the depth map and then select the pixel that has the highest intensity in the sample input hazy image and the selected brightest pixel is considered as atmospheric light.

Step 6: Calculate the transmission map using Eq. (11).

Step 7: Find haze free image using Eqs. (12) and (13).

Step 8: Image quality assessment (IQA) is done to check the quality of output haze free image. Terms found in IQA are MSE using Eq. (14), RMSE using Eq. (15), PSNR using Eq. (16), MSSIM using Eq. (21) and UQI using Eq. (20) with condition:  $T_1 = T_2 = T_3 = 0$  and  $\alpha = \beta = \gamma = 1$ .

Step 9: To increase the readability property of output haze free image, a simplest color balance algorithm is applied which gives our final better readable output image.

## 4 Experimental Results Evaluation

In order to demonstrate the productivity and effectiveness of the proposed method, this method is tested on various hazy images and the authors compared it with the methods of He et al. [12] and Zhu et al. [11]. The environment used for the implementation is Matlab2015a on a Pentium 4-3.3 GHz PC with 4 GB RAM. For showing proper and effective results the authors have taken general outdoor images and synthetic hazy images. Fig. 7 shows the results based on the proposed method, including depth map, refine depth map, transmission map, atmospheric light position and haze free image. The general outdoor images are taken from Google images, Flickr and the synthetic images are taken from the D-HAZY dataset.

The authors compared the proposed method with different methods which are shown in Fig. 8. It can be observed that the results of He et al. [12] are deviating from the ground truth image and also the color distortions happen. Zhu et al. [11] provide much better results but on the grounds of homogeneous scattering coefficient which does not happen in real atmosphere. In the proposed method, the usage of the scattering coefficient is done in accordance to the inhomogeneous atmosphere that actually happens in real atmosphere. For showing a clearer comparison between these methods, Tabs. 1–4 show the analysis of the image quality containing MSE, RMSE, PSNR, MSSIM and the UQI.

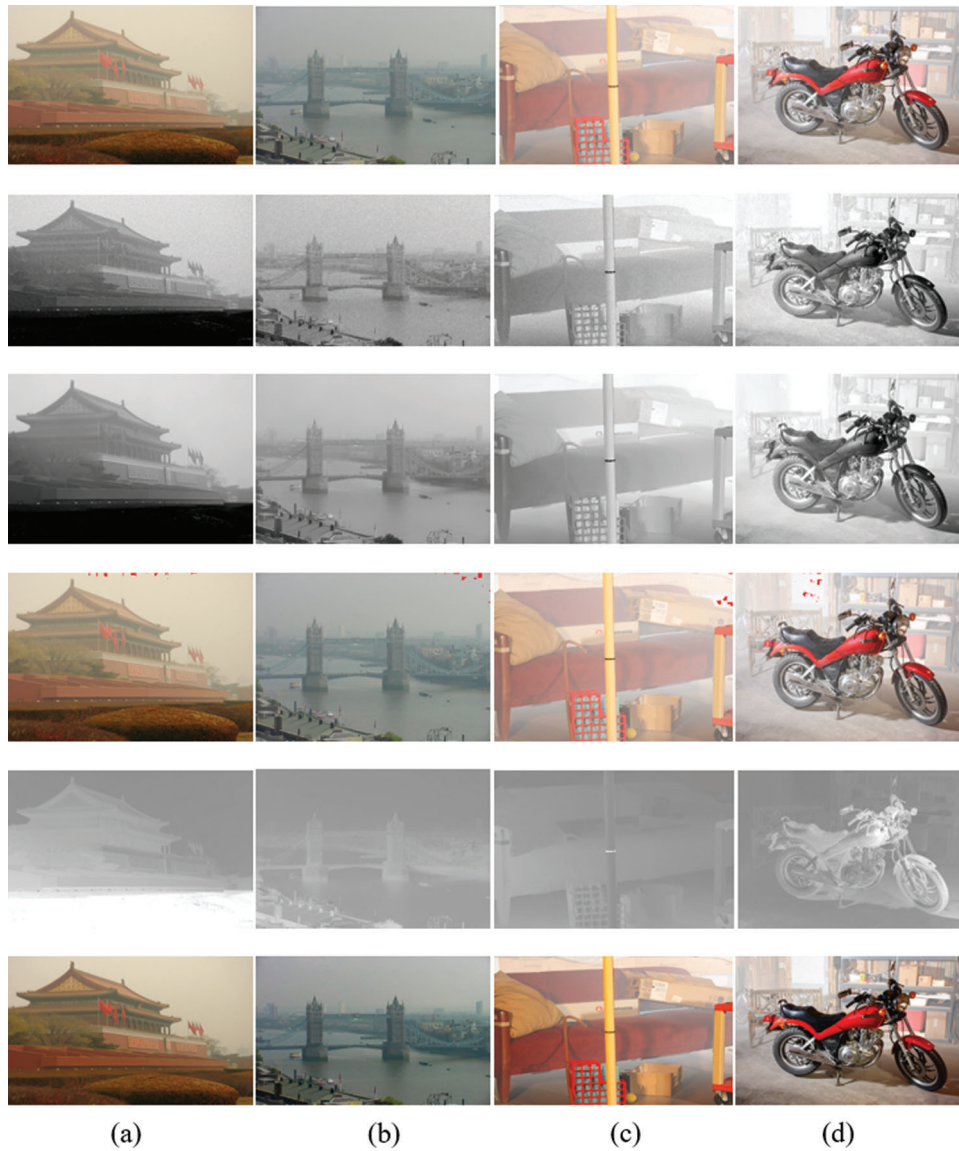


**Figure 7:** (a) and (b) General outdoor images (c) and (d) Synthetic hazy

Hence it is observed that the proposed method performs better than He et al. [12] and Zhu et al. [11] methods. Therefore we can say that making scattering coefficient flexible or variable according to inhomogeneous atmosphere we can achieve the results that are near to ground truth images and that give better image quality assessment parameters.

#### ***4.1 Post Processing Results of Haze Free Images***

It can be observed that the proposed method is quite successful to create a good haze free image but due to the scattered rays from the scene points do not reach the imaging system properly, the colors of the image get disturbed. So to make the color balance in haze free, the authors implemented Simple Color Balance Algorithm that balances the color of image on the basis of histogram of RGB color channels images [46].

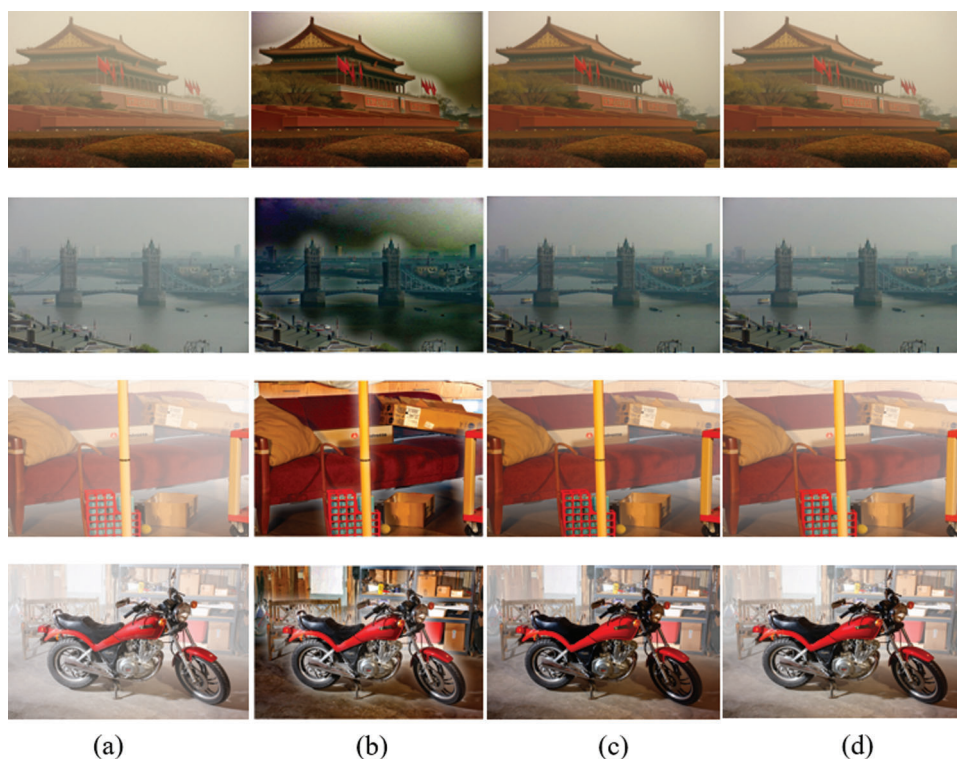


**Figure 8:** Comparison made on different methods by real world and synthetic images. (a) Sample hazy images (b) He et al. results [12] (c) Zhu et al. results [11] (d) Proposed method results

**Table 1:** Hazy image 1

| Methods         | MSE    | RMSE   | PSNR    | MSSIM  | UQI    |
|-----------------|--------|--------|---------|--------|--------|
| He et al.       | 0.2290 | 0.4785 | 26.8744 | 0.8980 | 0.5164 |
| Zhu et al.      | 0.0524 | 0.2289 | 39.4430 | 0.9974 | 0.8354 |
| Proposed method | 0.0217 | 0.1474 | 48.0617 | 0.9989 | 0.9237 |

**Table 2:** Hazy image 2

| Methods         | MSE    | RMSE   | PSNR    | MSSIM  | UQI    |
|-----------------|--------|--------|---------|--------|--------|
| He et al.       | 0.3752 | 0.6126 | 23.1623 | 0.8060 | 0.3796 |
| Zhu et al.      | 0.0642 | 0.2534 | 43.9705 | 0.9969 | 0.8185 |
| Proposed method | 0.0260 | 0.1611 | 48.9271 | 0.9988 | 0.9190 |

From Fig. 9, it can be analyzed that each haze free image is color balanced by Color Balance Algorithm by correcting the original histogram of RGB color channels of the images and the output image is better and its readability property has increased.

**Table 3:** Hazy image 3

| Methods         | MSE    | RMSE   | PSNR    | MSSIM  | UQI    |
|-----------------|--------|--------|---------|--------|--------|
| He et al.       | 0.5427 | 0.7367 | 22.9337 | 0.7283 | 0.4105 |
| Zhu et al.      | 0.2179 | 0.4608 | 27.4708 | 0.9897 | 0.7346 |
| Proposed method | 0.0642 | 0.2533 | 38.8634 | 0.9970 | 0.8992 |

**Table 4:** Hazy image 4

| Methods         | MSE    | RMSE   | PSNR    | MSSIM  | UQI    |
|-----------------|--------|--------|---------|--------|--------|
| He et al.       | 0.4110 | 0.6411 | 22.7229 | 0.8550 | 0.5686 |
| Zhu et al.      | 0.2130 | 0.4616 | 27.4763 | 0.9903 | 0.6742 |
| Proposed Method | 0.0650 | 0.2550 | 38.6276 | 0.9970 | 0.8709 |

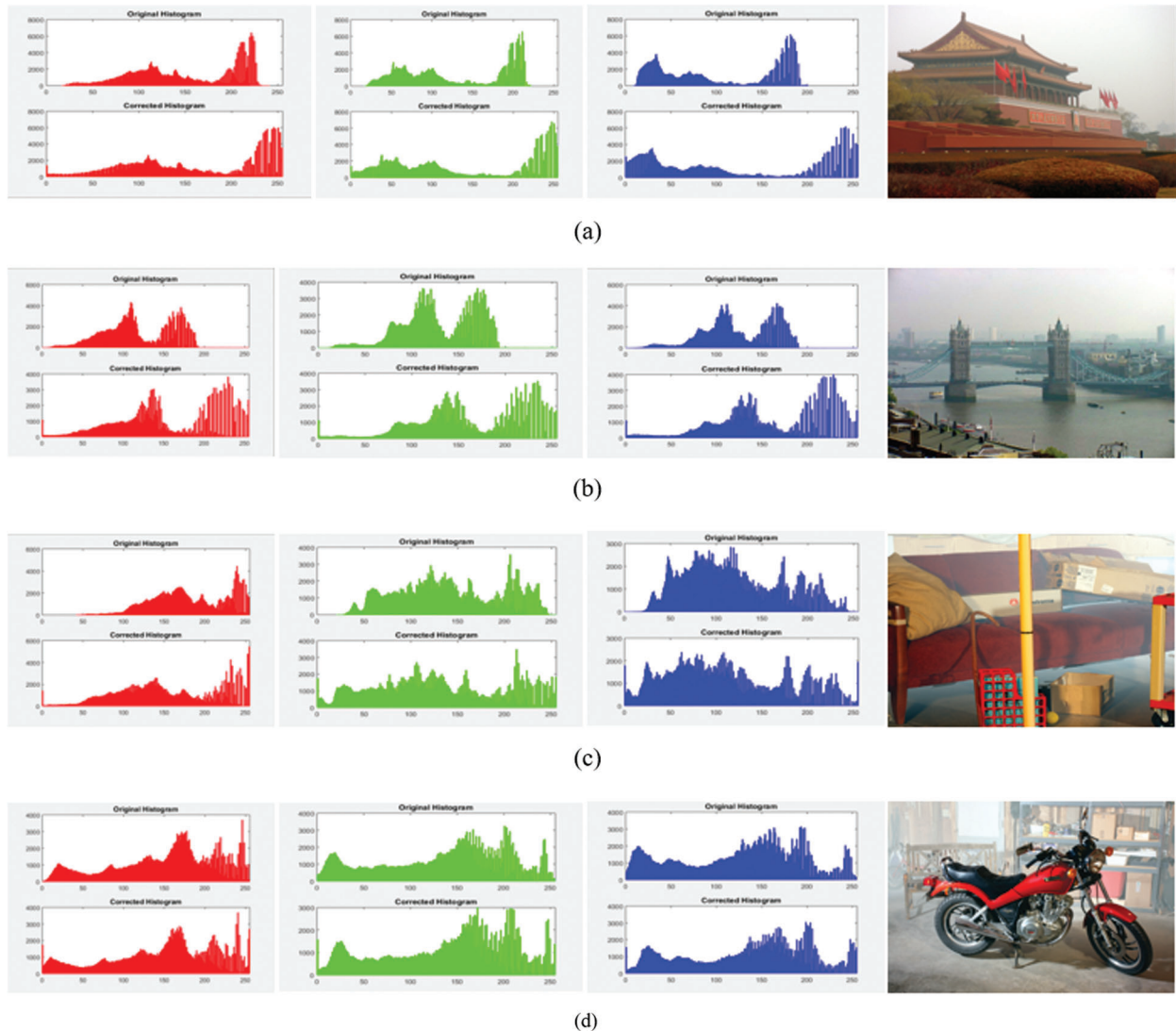


**Figure 9:** Post processing images (a) Haze free image 1 (b) Haze free image 2 (c) Haze free image 3 (d) Haze free image 4

## 5 Conclusion

In this paper, initially the authors have used the weighted guided image filtering to eliminate the drawbacks of guided image filtering. Afterwards the scattering coefficient is made variable according to inhomogeneous atmosphere and then the simplest color balance algorithm is applied for increasing the readability property of images. Experimental results show that the proposed method is better and more efficient than other methods.

Although the method that is proposed is efficient there is a problem that has to be solved. As the concentration of haze or other pollutants effects increased, such as fog, smog, then this method does not work properly. For addressing this problem, the authors will continue with the development of fusion based method that may minimize the loss of the image structure by a multistage strategy.

**Funding Statement:** The authors received no specific funding for this study.

**Conflicts of Interest:** The authors declare that they have no conflicts of interest to report regarding the present study.

## References

1. Ghazvini, A., Abdullah, S. N. H. S., Ayob, M. A. (2019). Recent trend in individual counting approach using deep network. *International Journal of Interactive Multimedia and Artificial Intelligence*, 5(5), 7–14. DOI 10.9781/ijimai.2019.04.003.
2. Jha, S., Dey, A., Kumar, R., Kumar-Solanki, V. (2019). A novel approach on visual question answering by parameter prediction using faster region based convolutional neural network. *International Journal of Interactive Multimedia and Artificial Intelligence*, 5(5), 30–37. DOI 10.9781/ijimai.2018.08.004.
3. Li, Z., Li, L., Yan, K., Zhang, C. (2017). Automatic image annotation using fuzzy association rules and decision tree. *Multimedia Systems*, 23(6), 679–690. DOI 10.1007/s00530-016-0530-9.
4. Jalal, A., Kamal, S. (2019). Improved behavior monitoring and classification using cues parameters extraction from camera array images. *International Journal of Interactive Multimedia and Artificial Intelligence*, 5(5), 71–78. DOI 10.9781/ijimai.2017.07.003.
5. Wang, H., Zhao, D., Ma, H. (2017). Informative image selection for crowdsourcing-based mobile location recognition. *Multimedia Systems*, 25(5), 513–523. DOI 10.1007/s00530-017-0562-9.
6. Min, W., Jiang, S., Wang, S., Xu, R., Cao, Y. et al. (2017). A survey on context-aware mobile visual recognition. *Multimedia Systems*, 23(6), 647–665. DOI 10.1007/s00530-016-0523-8.
7. González García, C., Núñez-Valdez, E., García-Díaz, V., Pelayo G-Bustelo, C., Cueva-Lovelle, J. M. (2019). A review of artificial intelligence in the internet of things. *International Journal of Interactive Multimedia and Artificial Intelligence*, 5(4), 9–20. DOI 10.9781/ijimai.2018.03.004.
8. Wang, W., Yuan, X. (2017). Recent advances in image dehazing. *IEEE/CAA Journal of Automaticasínica*, 4(3), 410–436.
9. Oakley, J. P., Satherley, B. L. (1998). Improving image quality in poor visibility conditions using a physical model for contrast degradation. *IEEE Transactions on Image Processing*, 7(2), 167–179. DOI 10.1109/83.660994.
10. Gibson, K. B., Belongie, S. J., Nguyen, T. Q. (2013). Example based depth from fog. *IEEE International Conference on Image Processing, Melbourne, VIC, Australia, 2013*, 728–732.
11. Zhu, Q., Mai, J., Shao, L. (2015). A fast single image haze removal algorithm using color attenuation prior. *IEEE Transactions on Image Processing*, 24(11), 3522–3533. DOI 10.1109/TIP.2015.2446191.
12. He, K., Sun, J., Tang, X. (2011). Single image haze removal using dark channel prior. *IEEE Transactions on Pattern Analysis and Machine Intelligence*, 33(12), 2341–2353. DOI 10.1109/TPAMI.2010.168.
13. Wang, Q., Ward, R. K. (2007). Fast image/video contrast enhancement based on weighted thresholded histogram equalization. *IEEE Transactions on Consumer Electronics*, 53(2), 757–764. DOI 10.1109/TCE.2007.381756.

14. Dale-Jones, R., Tjahjadi, T. (1993). A study and modification of the local histogram equalization algorithm. *Pattern Recognition*, 26(9), 1373–1381. DOI 10.1016/0031-3203(93)90143-K.
15. Khan, M. F., Khan, E., Abbasi, Z. A. (2014). Segment dependent dynamic multi-histogram equalization for image contrast enhancement. *Digital Signal Processing*, 25, 198–223. DOI 10.1016/j.dsp.2013.10.015.
16. Celik, T., Tjahjadi, T. (2011). Contextual and variational contrast enhancement. *IEEE Transactions on Image Processing*, 20(12), 3431–3441. DOI 10.1109/TIP.2011.2157513.
17. Land, E. H., McCann, J. J. (1971). Lightness and retinex theory. *Journal of the Optical Society of America*, 61(1), 1–11. DOI 10.1364/JOSA.61.000001.
18. Cooper, T. J. (2004). Analysis and extensions of the Frankle-McCann Retinex algorithm. *Journal of Electronic Imaging*, 13(1), 85. DOI 10.1117/1.1636182.
19. Jobson, D. J., Rahman, Z., Woodell, G. A. (1997). Properties and performance of a center/surround retinex. *IEEE Transactions on Image Processing*, 6(3), 451–462. DOI 10.1109/83.557356.
20. Rahman, Z., Jobson, D. J., Woodell, G. A. (1996). Multi-scale retinex for color image enhancement. *Proceedings of 3rd IEEE International Conference on Image Processing, Lausanne, Switzerland*, 3, 1003–1006.
21. Seow, M. J., Asari, V. K. (2006). Ratio rule and homomorphic filter for enhancement of digital colour image. *Neurocomputing*, 69(7), 954–958. DOI 10.1016/j.neucom.2005.07.003.
22. Grewe, L. L., Brooks, R. R. (1998). Atmospheric attenuation reduction through multisensor fusion. *Proceedings of SPIE Sensor Fusion: Architectures, Algorithms and Applications II, International Society for Optics and Photonics*, 3376, 102–109.
23. Starck, J. L., Murtagh, F., Candes, E. J., Donoho, D. L. (2003). Gray and color image contrast enhancement by the curvelet transform. *IEEE Transactions on Image Processing*, 12(6), 706–717. DOI 10.1109/TIP.2003.813140.
24. Verma, M., Kaushik, V. D., Pathak, V. K. (2015). An efficient deblurring algorithm on foggy images using curvelet transforms. *Proceedings of the Third International Symposium on Women in Computing and Informatics, Kochi, India, ACM*, 426–431.
25. Schaul, L., Fredembach, C., Susstrunk, S. (2009). Color image dehazing using the near-infrared. *16th IEEE International Conference on Image Processing, Cairo, Egypt, IEEE*, 1629–1632.
26. Ancuti, C. O., Ancuti, C., Bekaert, P. (2010). Effective single image dehazing by fusion. *IEEE International Conference on Image Processing, Hong Kong, China*, 3541–3544.
27. Ancuti, C. O., Ancuti, C. (2013). A single image dehazing by multi-scale fusion. *IEEE Transactions on Image Processing*, 22(8), 3271–3282. DOI 10.1109/TIP.2013.2262284.
28. Ancuti, C. O., Ancuti, C., Hermans, C., Bekaert, P. (2011). Image and video decolorization by fusion. In: Kimmel, R., Klette, R., Sugimoto, A. (eds.) *Asian Conference on Computer Vision—ACCV 2010, Berlin, Heidelberg, Springer*, vol. 6492, 79–92.
29. Narasimhan, S. G., Nayar, S. (2003). Interactive deweathering of an image using physical models. *IEEE Workshop on Color and Photometric Methods in Computer Vision, in conjunction with ICCV, France*, 6(4), 1–24.
30. Tang, K., Yang, J., Wang, J. (2014). Investigating haze-relevant features in a learning framework for image dehazing. *IEEE Conference on Computer Vision and Pattern Recognition, 2014*, 2995–3002.
31. Schechner, Y. Y., Narasimhan, S. G., Nayar, S. (2001). Instant dehazing of images using polarization. *Proceedings of the 2001 IEEE Computer Society Conference on Computer Vision and Pattern Recognition, Kauai, HI, USA*, 1, I-325–I-332.
32. Nayar, S. K., Narasimhan, S. G. (1999). Vision in bad weather. *Proceedings of the Seventh IEEE International Conference on Computer Vision, Kerkyra, Greece*, 2, 820–827.
33. Narasimhan, S. G., Nayar, S. K. (2000). Chromatic framework for vision in bad weather. *Proceedings IEEE Conference on Computer Vision and Pattern Recognition, Hilton Head Island, SC, USA*, 1, 598–605.
34. Narasimhan, S. G., Nayar, S. K. (2002). Vision and the atmosphere. *International Journal of Computer Vision*, 48(3), 233–254. DOI 10.1023/A:1016328200723.
35. Narasimhan, S. G., Nayar, S. K. (2003). Contrast restoration of weather degraded images. *IEEE Transactions on Pattern Analysis and Machine Intelligence*, 25(6), 713–724. DOI 10.1109/TPAMI.2003.1201821.

36. Narasimhan, S. G., Nayar, S. K. (2001). Removing weather effects from monochrome images. *Proceedings of the 2001 IEEE Computer Society Conference on Computer Vision and Pattern Recognition, Kauai, HI, USA, 2*, 186–193.
37. Tan, R. T. (2008). Visibility in bad weather from a single image. *IEEE Conference on Computer Vision and Pattern Recognition, Anchorage, AK, USA, 2008*, 1–8.
38. Fattal, R. (2008). Single image dehazing. *ACM Transactions on Graphics, 27(3)*, 1–9. DOI 10.1145/1360612.1360671.
39. Kratz, L., Nishino, K. (2009). Factorizing scene albedo and depth from a single foggy image. *IEEE 12th International Conference on Computer Vision, Kyoto, Japan, 2009*, 1701–1708.
40. Tarel, J. P., Hautiere, N. (2009). Fast visibility restoration from a single color or gray level image. *IEEE 12th International Conference on Computer Vision, Kyoto, Japan, 2009*, 2201–2208.
41. Kim, J. H., Jang, W. D., Sim, J. Y., Kim, C. S. (2013). Optimized contrast enhancement for real-time image and video dehazing. *Journal of Visual Communication and Image Representation, 24(3)*, 410–425. DOI 10.1016/j.jvcir.2013.02.004.
42. Kim, J. H., Sim, J. Y., Kim, C. S. (2011). Single image dehazing based on contrast enhancement. *2011 IEEE International Conference on Acoustics, Speech and Signal Processing, Prague, Czech Republic*, 1273–1276.
43. Zhu, Q. S., Mai, J. M., Shao, L. (2014). Single image dehazing using color attenuation prior. *Proceedings 25th British Machine Vision Conference*, 1–10.
44. Li, Z., Zheng, J., Zhu, Z., Yao, W., Wu, S. (2015). Weighted guided image filtering. *IEEE Transactions on Image Processing, 24(1)*, 120–129. DOI 10.1109/TIP.2014.2371234.
45. Wang, Z., Bovik, A. C., Sheikh, H. R., Simoncelli, E. P. (2004). Image quality assessment: from error visibility to structural similarity. *IEEE Transactions on Image Processing, 13(4)*, 600–612. DOI 10.1109/TIP.2003.819861.
46. Limare, N., Lisani, J. L., Morel, J. M., Petro, A. B., Sbert, C. (2011). Simplest color balance. *Image Processing on Line, 1*, 297–315.
47. Kapoor, R., Gupta, R., Kumar, R., Jha, S. (2019). Fog removal in images using improved dark channel prior and contrast limited adaptive histogram equalization. *Multimedia Tools and Applications, 78(16)*, 23281–23307. DOI 10.1007/s11042-019-7574-8.
48. Sabharwal, T., Gupta, R. (2019). Human identification after plastic surgery using region based score level fusion of local facial features. *Journal of Information Security and Applications, 48*, 102373. DOI 10.1016/j.jisa.2019.102373.
49. Hernández, F. L., de Ory, E. G., Aguilar, S. R., Crespo, R. G. (2018). Residue properties for the arithmetical estimation of the image quantization table. *Applied Soft Computing, 67*, 309–321. DOI 10.1016/j.asoc.2018.03.017.
50. Khari, M., Garg, A. K., Crespo, R. G., Verdú, E. (2019). Gesture recognition of RGB and RGB-D static images using convolutional neural networks. *International Journal of Interactive Multimedia & Artificial Intelligence, 5(7)*, 22–27.
51. Gupta, R., Khari, M., Gupta, D., Crespo, R. G. (2020). Fingerprint image enhancement and reconstruction using the orientation and phase reconstruction. *Information Sciences*.
52. Pacheco, A., Baron, H. B., Crespo, R. G., Espada, J. P. (2014). Reconstruction of high resolution 3D objects from incomplete images and 3D information. *International Journal of Interactive Multimedia and Artificial Intelligence, 2(6)*, 7–16. DOI 10.9781/ijimai.2014.261.
53. Hemeida, A. M., Mansour, R., Hussein, M. E. (2019). Multilevel thresholding for image segmentation using an improved electromagnetism optimization algorithm. *International Journal of Interactive Multimedia and Artificial Intelligence, 5(4)*, 102–112. DOI 10.9781/ijimai.2018.09.001.
54. Dua, M., Gupta, R., Khari, M., Crespo, R. G. (2019). Biometric iris recognition using radial basis function neural network. *Soft Computing, 23(22)*, 11801–11815. DOI 10.1007/s00500-018-03731-4.